Crystal growth of the Nowotny chimney ladder phase Fe_2Ge_3 : exploring new Fe-based narrow-gap semiconductor with promising thermoelectric performance

Crystal Growth of the Nowotny Chimney Ladder Phase Fe_2Ge_3: Exploring New Fe-Based Narrow-Gap Semiconductor with Promising Thermoelectric Performance

Valeriy Yu. Verchenko[1,2,*], Zheng Wei[3], Alexander A. Tsirlin[4], Carolien Callaert[5], Anton Jesche[4], Joke Hadermann[5], Evgeny V. Dikarev[3], and Andrei V. Shevelkov[1]

[1]Department of Chemistry, Lomonosov Moscow State University, 119991 Moscow, Russia

[2]National Institute of Chemical Physics and Biophysics, 12618 Tallinn, Estonia

[3]Department of Chemistry, University at Albany, SUNY, Albany, 12222 New York, United States

[4]Experimental Physics VI, Center for Electronic Correlations and Magnetism, Institute of Physics, University of Augsburg, 86135 Augsburg, Germany

[5]EMAT, University of Antwerp, B-2020 Antwerp, Belgium

[*]e-mail: valeriy.verchenko@gmail.com

Abstract

A new synthetic approach based on chemical transport reactions has been introduced to obtain the Nowotny chimney ladder phase Fe_2Ge_3 in the form of single crystals and polycrystalline powders. The single crystals possess the stoichiometric composition and the commensurate chimney ladder structure of the Ru_2Sn_3 type in contrast to the polycrystalline samples that are characterized by a complex microstructure. In compliance with the 18-*n* electron counting rule formulated for T-E intermetallics, electronic structure calculations reveal a narrow-gap semiconducting behavior of Fe_2Ge_3 favorable for high thermoelectric performance. Measurements of transport and thermoelectric properties performed on the polycrystalline samples confirm the formation of a narrow band gap of ~ 30 meV and reveal high absolute values of the Seebeck coefficient at elevated temperatures. Low glass-like thermal conductivity is observed in a wide temperature range that might be caused by the underlying complex microstructure.

Introduction

Intermetallic compounds formed in binary systems T-E, where T is a transition metal, and E is a *p*-metal or metalloid, are known as T-E intermetallics or polar intermetallics. In these compounds, the chemical bonding deviates significantly from the simple metallic bonding provoking extended interest and comprehensive studies. On one hand, peculiarities of the chemical bonding in T-E intermetallics provide a background for unusual physical properties, especially in the electronic transport, giving rise to narrow-gap semiconductors,[1-6] high- and low-temperature thermoelectric materials[7-11] as well as superconductors.[12-14] This renders the T-E intermetallics promising functional materials for transport and thermoelectric applications. On the other hand, bonding between the T and E atoms in these compounds represents an intermediate case that can not be solely assigned to the limits of ionic, covalent or metallic bonding, thus markedly hindering its microscopic description and analysis. Recently, a unified picture of the chemical bonding in T-E intermetallics based on isolobal analogies to molecular T complexes began to take shape.[15] A new approach, the 18-*n* rule, has been formulated.[16] It considers the formation of multicenter bonds between the T and E atoms as a pathway to achieve the 18-electron configuration for each T atom. Currently, this rule successfully explains the stability of more than 34 different classes of T-E intermetallic compounds.[17]

The 18-*n* rule goes back to the studies of crystal and electronic structures of the Nowotny chimney ladder phases (NCLs). NCLs are a class of T-E intermetallics with the general formula T_tE_m known for their unique structural flexibility. In the crystal structure, *m*-step helices of E atoms are enclosed inside the 4-step helices of T atoms that form the tetragonal β-Sn-type arrangement. Helices of E atoms may be rather simple 2- or 3-step helices, or remarkably more complex ones leading to incommensurate modulations on top of the parent tetragonal structure. For NCLs, a set of empirical rules was established providing relations between stoichiometry, incommensurability of the crystal structure, and chemical bonding. According to the first rule,[18] the total number of valence electrons per T atom in a NCL compound is

equal or almost equal to 14. The second rule accounts for the appearance of pseudoperiodicity in the crystal structure with a spacing that is directly related to the stoichiometry and real periodicity of the compound, $c_{pseudo} = c/(2t\text{-}m)$.[19] Electronic structure calculations elucidate the first electron-counting rule in terms of the opening of a pseudogap or a real gap in the vicinity of the Fermi energy providing for an additional stability of NCLs.[18] Analysis of the band structure and chemical bonding reveals that such special electron count in the NCLs is connected with the formation of the 18-electron configuration of each T atom. Further, this rule was extended through the isolobal analogies to other intermetallic structure types leading to the more general 18-*n* rule.[17] Hereby, the Nowotny chimney ladder phases are at the origin of our understanding of chemical bonding in the T-E intermetallics. Despite the recent progress in this field, the NCLs are still compounds that give rise to puzzling questions regarding their crystal and electronic structures.

Recently, a new NCL compound was discovered in the binary system Fe-Ge.[20] This compound is thermodynamically stable only at relatively low temperatures below *ca.* 600 °C and remains hidden due to the kinetic inertness of iron and germanium at such temperatures. The Fe_2Ge_3 composition and Ru_2Sn_3 structure type were assumed by Gerasimov *et al.*[20] based on the data obtained for polycrystalline two-phase sample. However, neither the Rietveld refinement nor the proper indexing of the diffraction pattern was performed.[20] Later, Li *et al.*[21] performed transmission electron microscopy study on a sample prepared under the same conditions and found indications of an incommensurately modulated Nowotny chimney ladder structure with the composition $FeGe_\gamma$ deviating from the stoichiometric one with $\gamma = 1.5$. This incommensurability of the crystal structure presumably leads to a glass-like behavior characterized by the low thermal conductivity at high temperatures as proposed in a recent study by Sato *et al.*, who established $FeGe_\gamma$ as a promising thermoelectric material with the large power factor of 1.9 mW m^{-1} K^{-2} and the dimensionless figure-of-merit of 0.57 near 600 K.[22]

Herein, we put forward a synthetic approach based on chemical transport reactions that enables us to overcome the kinetic passivity of Fe and Ge at low

temperatures and to obtain high-quality polycrystalline samples as well as single crystals of the Nowotny chimney ladder phase Fe_2Ge_3. We thoroughly investigate the crystal structure of this compound using single-crystal X-ray diffraction, powder X-ray diffraction, and transmission electron microscopy. First-principles electronic structure calculations provide insight into chemical bonding in this NCL compound. Transport properties measured on polycrystalline samples are discussed along with details of the electronic structure.

Experimental Section

Synthesis of polycrystalline samples of $FeGe_\gamma$ was performed in two steps. First, Fe (powder, ≥ 99.99%, Sigma Aldrich) and Ge (chips, 99.999%, Sigma Aldrich) mixtures were prepared with a total mass of 0.5 g for the γ = 1.22; 1.35; 1.5; and 1.86 ratios that corresponds to 55; 57.5; 60 and 65 at.% Ge, respectively. The mixtures were placed inside quartz ampoules, which were evacuated to the residual pressure of 1×10^{-2} torr and sealed. The ampoules were annealed at 900 °C for 5 days in order to overcome the kinetic inertness of Fe and Ge through the use of high temperature. Then, the ampoules were cooled down to room temperature in the shut off furnace. The obtained mixtures were grinded and annealed again at 700 °C for 7 days. Phase analysis using powder X-ray diffraction (PXRD) technique shows that for each value of γ the mixture of FeGe (*P*6/*mmm*, CoSn-type) and $FeGe_2$ (*I*4/*mcm*, $CuAl_2$-type) is formed at the first step. Second, the pre-synthesized mixtures were placed into quartz ampoules together with 5 mg of I_2 crystals, which were purified by sublimation prior to the use. Ampoules were evacuated and sealed, annealed at 480 °C for 7 days, and cooled down to room temperature in the shut off furnace. After that, the samples were grinded again in an agate mortar, and subsequently annealed at 500 °C for another 7 days.

Growth of single crystals of Fe_2Ge_3 was performed using chemical-transport reactions. The pre-synthesized stoichiometric mixture of FeGe (*P*6/*mmm*, CoSn-type) and $FeGe_2$ (*I*4/*mcm*, $CuAl_2$-type) with a total mass of 0.5 g was loaded into a quartz ampoule together with I_2 and $Mo(CO)_6$ (1 and 3 $mg\cdot cm^{-3}$ per volume of the ampoule, respectively) as transport agents. The ampoule with length of 7 cm and inner diameter of 0.8 cm was sealed under the residual pressure of 1×10^{-2} torr, and annealed in a two-zone horizontal furnace having a temperature gradient along the tube. The starting mixture was placed at 480 °C, while the crystallization zone was kept at 450 °C for one week yielding a nonequilibrium mixture that contains well-shaped crystals of Fe_2Ge_3.

Characterization of samples was performed by the following techniques. The obtained powders and single crystals were analyzed using a scanning electron

microscope JSM JEOL 6490-LV equipped with energy-dispersive X-ray (EDX) analysis system INCA x-Sight. For quantitative analysis of the elemental composition, external standards provided by MAC Analytical Standards were used. Powder X-ray diffraction (PXRD) patterns were registered on a Bruker D8 Advance diffractometer (LynXEye detector, Cu source, no monochromator used, λ = 1.5418 Å). The sample with γ = 1.50 was measured with the use of monochromatic radiation (Ge monochromator, λ = 1.540598 Å). Single crystals were investigated using a Bruker D8 Venture single crystal X-ray diffractometer (PHOTON 100 CMOS detector, Mo source, graphite monochromator, λ = 0.73071 Å). The absorption correction was performed using the multi-scan routine (SADABS program).[23] The crystal structure was solved by direct methods and subsequently refined against $|F^2|$ in the full-matrix anisotropic approximation using the SHELX-2016/6 program package.[24] For the transmission electron microscopy (TEM) study, the powder samples were crushed, dissolved in ethanol and put on a Cu grid. The data were acquired on a Technai G2, on a Phillips CM 20, and on a FEI Titan aberration-corrected transmission electron microscope using double tilt holders. The HAADF-STEM simulation was performed using the MULTEM software package.[25]

Electronic structure calculations were performed within the framework of density functional theory (DFT) using Full-Potential Local-Orbital minimum basis band-structure FPLO code[26] (version 14.00-47). In the scalar relativistic regime, local density approximation (LDA) was used to treat the exchange-correlation energy.[27] Integrations in the *k*-space were performed by an improved tetrahedron method[28] on a grid of 24×24×24 *k*-points. Spin-polarized calculations were performed within the LSDA formalism on a grid of 12×12×12 *k*-points using the ferromagnetic and antiferromagnetic initial spin configurations. In the latter configuration, the Fe1 atom has a spin-up direction of moment, while the Fe2 and Fe3 atoms possess spin-down moments. All moments are aligned along the (001) direction of the unit cell.

Magnetic properties were measured on a collection of 11 single crystals of Fe_2Ge_3 with a total mass of 95(15) μg grown by chemical transport method. Magnetization was registered using a superconducting quantum interference device

(SQUID) magnetometer of the Magnetic Property Measurement System (MPMS 3, Quantum Design) at temperatures between 2 K and 300 K in external magnetic field of 7 T.

Transport properties were measured on pellets pressed from the $FeGe_{\gamma}$ powder at external pressure of 100 bar at room temperature. In these conditions, the relative density of 85 % has been achieved. Resistivity and thermoelectric properties were measured on rectangular-shaped pellets with typical dimensions of $0.8 \times 0.3 \times 0.2$ cm^3 using Resistivity and Thermal Transport options of the Physical Property Measurement System (PPMS, Quantum Design), respectively, at temperatures between 2 K and 400 K in zero magnetic field.

Results and Discussion

Chemical transport

Regarding the thermodynamic and kinetic properties of alloys in the Fe-Ge system, the existence of several binary phases, including *β*-phase, *η*-phase, Fe_6Ge_5, FeGe, and $FeGe_2$, is envisaged in the Ge-rich part of the phase diagram[29] (Figure 1). Kinetic properties play a central role in the system, since kinetic inertness of iron and germanium prevents the formation of compounds at temperatures below *ca.* 700 °C. Therefore, synthesis of the listed compounds requires activation of the iron-germanium interaction, and different routes can be employed for this purpose, among which thermal activation is the most commonly used. For instance, the mixture of Fe and Ge can be activated by sintering in a high-frequency furnace, by employing the arc-melting technique, or simply by annealing in the evacuated quartz ampoule at 1000 °C or higher.[30] Starting from the activated mixture, binary compounds can be synthesized, usually by the long-duration annealing of alloys at lower temperatures. The above synthetic approach based on thermal activation and post-annealing leads to the formation of thermodynamically stable compounds. Moreover, decomposition of such compounds, if allowed by phase relations, is usually hindered due to kinetic reasons, thus screening other binary compounds that are stable at low temperatures. The latter explains why the Fe_2Ge_3 phase, which is stable below 580 °C, remained undiscovered due to the high thermodynamic and kinetic stability of FeGe and $FeGe_2$. In fact, Fe_2Ge_3 can not be synthesized even by the long-duration annealing of the activated mixture of Fe and Ge below 580 °C, because the mixture is kinetically stable. Our results show that not even traces of the Fe_2Ge_3 phase could be detected in the synthesis products. Therefore, synthesis of Fe_2Ge_3 requires alternative routes that are applicable at temperatures below 580 °C.

Among such routes, the synthesis under pressure, activation by milling, or chemical transport reactions can be employed to enhance the iron-germanium interaction at low temperatures. Indeed, Gerasimov *et al.* obtained the new compound as a side product by employing the ball-milling procedure.[20] The authors conducted differential scanning calorimetry study on the $FeGe_2$ sample that was exposed to ball-

milling, and unexpectedly found two endothermic effects on the DSC curve at temperatures below 700 °C. They assigned the effect at 580 °C to the decomposition of a previously unknown phase that was roughly identified as "Fe_2Ge_3". According to Gerasimov *et al.*, the Fe-Ge phase diagram additionally contains the Fe_2Ge_3 phase, which is stable at the temperatures below 580 °C, as shown in Figure 1. According to Li *et al.*,[21] the new phase Fe_2Ge_3 should rather be considered as $FeGe_\gamma$, implying the incommensurability of the crystal structure and possible off-stoichiometry ($\gamma \neq 1.5$). Hereafter, we will refer to the polycrystalline samples as $FeGe_\gamma$ and to the case of the ideal chimney ladder structure as Fe_2Ge_3, for clarity.

In addition to the mechanochemical synthesis,[20,21] Sato *et al.* introduced spark plasma sintering under pressure to obtain the bulk samples of $FeGe_\gamma$ with higher relative density.[22] Summarizing the synthetic aspects, we can underline that only mechanical activation was used previously to enhance the Fe-Ge interaction at low temperatures. This method of activation, combined with post annealing or spark plasma sintering at temperatures below 500 °C, leads to the formation of polycrystalline $FeGe_\gamma$ that was found to possess the complex, hitherto unsolved incommensurately modulated crystal structure. Difficulties in interpretation of the crystal structure of $FeGe_\gamma$ are also connected with the presence of admixtures, owing to the lack of precise control over the elemental composition of samples prepared by ball-milling and post-treatment. In order to improve the synthesis of $FeGe_\gamma$ and to obtain single crystals of the new compound, we introduced the chemical transport method that facilitates the Fe-Ge interaction at low temperatures.

We started with the thermal activation of the Fe-Ge mixtures using the standard ampoule technique. High-temperature annealing of the Fe-Ge samples with compositions in the range between 50 and 66.7 at.% Ge leads to the formation of FeGe (*P*6/*mmm*, CoSn-type) and $FeGe_2$ (*I*4/*mcm*, $CuAl_2$-type) according to the PXRD results. On the phase diagram (Figure 1), there are two phase fields adjacent to the desired Fe_2Ge_3 composition. The first field between 50 and 60 at.% Ge at temperatures below 580 °C corresponds to coexisting FeGe and Fe_2Ge_3, while the second field at temperatures below 530 °C with compositions from 60 up to 100 at.%

Ge is represented by the equilibrium mixture of Fe_2Ge_3 and Ge. The samples with γ = 1.22 and 1.35 fall into the first field, while the sample with γ = 1.86 is in the second field, and the stoichiometric composition γ = 1.5 is in between the two areas. According to the PXRD results, which are shown in Figure 2, the phase compositions of samples is in full agreement with the proposed phase relations. Indeed, the samples with γ = 1.22 and 1.35 contain the chimney ladder phase $FeGe_\gamma$ and FeGe ($P2_13$, FeSi-type). The amount of the latter increases with decreasing γ. At the same time, the sample with γ = 1.86 contains elemental germanium and $FeGe_\gamma$. It should be noted that peak positions of the $FeGe_\gamma$ phase slightly change with γ, indicating a narrow homogeneity range of the compound. The sample with the stoichiometric composition γ = 1.5 is represented primarily by the desired chimney ladder phase $FeGe_\gamma$ with minor amounts of the FeGe admixture ($P2_13$, FeSi-type). The appearance of a secondary phase in this sample again can be explained by a narrow homogeneity range for the $FeGe_\gamma$ phase.

The choice of iodine as transport agent is motivated by the following reasons. Iodine had been successfully used for preparation of different Fe-Ge compounds by the chemical transport method,[30] because it reversibly forms volatile compounds with Fe and Ge. The following chemical transport reactions are proposed:

$$3Fe + 4I_2 \leftrightarrow Fe_3I_8,$$

$$Ge + 2I_2 \leftrightarrow GeI_4.$$

Note that Fe_3I_8 is only a conjectural product. It contains both the Fe(II) and Fe(III) species underlining that the formation of Fe(III) is responsible for the chemical transport of iron at temperatures below *ca.* 600 °C.[31] The formation of Fe_2Ge_3 from the equimolar mixture of FeGe and $FeGe_2$ can be written as:

$$3FeGe + 3FeGe_2 + 26I_2 \leftrightarrow 2Fe_3I_8 + 9GeI_4 \leftrightarrow 3Fe_2Ge_3 + 26I_2.$$

Among the volatile products, GeI_4 has the highest equilibrium vapor-pressure at temperatures above 350 °C. At the same time, the volatility of Fe_3I_8 is not high at 400-500 °C. However, its partial pressure is high enough to initiate the chemical transport, and we found that the addition of iodine to the reaction mixture leads to the formation of the desired compound at 500 °C. The synthesis leads to polycrystalline

$FeGe_\gamma$ with the size of crystallites typically in the range of 0.2-4 μm. Presumably, nucleation is the rate-determining step of the process, and the formation of larger crystals is not observed in the reaction. Therefore, the chemical transport method with the choice of iodine as transport agent can be successfully utilized for the preparation of polycrystalline $FeGe_\gamma$ on a par with the ball-milling technique. Moreover, the developed synthetic approach involves only the ampoule technique and does not require any special equipment, it is time-saving and easy to implement.

Furthermore, we continued developing the chemical transport method in order to obtain single crystals. To this end, we attempted experiments in the temperature gradient. However, we quickly realized that no transport occurs below 500 °C. Chemical transport in the temperature gradient 480-450 °C with the addition of iodine leads to the formation of a nonequilibrium mixture of the cubic FeGe ($P2_13$, FeSi-type) and hexagonal FeGe ($P6/mmm$, CoSn-type) in the heating zone, and elemental germanium in the crystallization zone. The formation of Ge among the products indicates that the partial vapor-pressure of the Fe-containing component is not sufficient. In order to improve the transport of Fe through the vapor phase, we chose $Mo(CO)_6$ as an additional transport agent. Molybdenum hexacarbonyl $Mo(CO)_6$ is a crystalline compound stable at room temperature that sublimates readily upon slight heating under vacuum. It decomposes according to the reaction $Mo(CO)_6 \rightarrow Mo(CO)_y + (6-y)CO$ forming the nonvolatile $Mo(CO)_y$ polymetallic clusters ($y < 6$) in the hot zone and providing the CO vapor for the chemical transport.[32] The following chemical transport reactions may occur during the synthesis of Fe_2Ge_3 with the use of I_2 and $Mo(CO)_6$ as transport agents:

$$3FeGe + 3FeGe_2 + 15CO + 22I_2 \leftrightarrow Fe_3I_8 + 3Fe(CO)_5 + 9GeI_4 \leftrightarrow 3Fe_2Ge_3 + 15CO + 22I_2.$$

The use of I_2 together with $Mo(CO)_6$ led to appearance of new single crystals with typical sizes in the range of 100-750 μm in the crystallization zone. According to the EDXS results, these crystals contain 40.2(7) at.% Fe and 59.8(8) at.% Ge close to the stoichiometric composition $FeGe_\gamma$ with $\gamma = 1.5$. Further, single-crystal XRD

experiments revealed the chimney ladder structure confirming that the desired compound was obtained.

Summarizing all of the above, the method of chemical transport can be efficiently employed to obtain polycrystalline samples of $FeGe_\gamma$ at the isothermal conditions with the use of iodine as transport agent. In this case, chemical transport reactions activate decomposition of $FeGe_2$ and FeGe, and facilitate the Fe-Ge interaction, thus eliminating kinetic barriers in the Fe-Ge system. In the temperature gradient with concomitant application of I_2 and $Mo(CO)_6$ as transport agents, single crystals can be obtained.

Crystal structure: polycrystals

The PXRD pattern of $FeGe_\gamma$ for γ = 1.5 presented in Figure 2 can not be indexed neither in the primitive tetragonal lattice that is expected for the Ru_2Sn_3-type of crystal structure[33] nor in the orthorhombic system expected for the Ru_2Ge_3-type chimney ladder phase.[34] Moreover, the observed reflections are shifted from the positions calculated for the idealized structure in a complex manner implying possible incommensurability, necessitating a TEM investigation of the polycrystalline samples of $FeGe_\gamma$.

According to the TEM results, an orthorhombic commensurate structure with cell parameters approximately $a \approx 5.45$ Å, $b \approx 5.6$ Å, and $c \approx 8.95$ Å is present in the sample. Representative selected area electron diffraction (SAED) patterns of this phase along the main zone axes are shown in Figure 3. Tilt series collected from different crystals allow to derive the reflection conditions 0*kl*: $l = 2n$; *h*0*l*: $l = 2n$; 00*l*: $l = 2n$; and *hkl*, *hk*0, *h*00, and 0*k*0: no conditions, which indicates extinction symbol *Pcc*- and allows two orthorhombic space groups, *Pcc*2 and *Pccm*. From SAED patterns alone, differentiation between these groups is not possible.

Further investigations show that the phase with the incommensurate structure is also present in the sample. The SAED patterns taken along the [1-10] and [100] directions (Figure 4a and 4b) can be indexed with cell parameters approximately $a \approx 5.6$ Å, $c \approx 4.6$ Å, and $q = 0.49(3)\, c^*$. With this *q*-vector, the [001] SAED patterns are indistinguishable from those of the commensurate phase (Figure 3c), because of the

absence of nonzero components along a^* and b^*. However, also slightly different q-vectors were found, as shown in Figure 4c and the bottom inset in Figure 4a, where the components along a^* and b^* differ from zero. The patterns in Figure 4a and 4b with q = 0.49(3) c^* are similar to those in Ref. [21], and are in agreement with the reflection conditions of the superspace group $I4_1/amd$:00ss proposed in literature for incommensurately modulated NCLs,[35] i.e. $hklm$: $h + k + l = 2n$, 0klm: $m = 2n$, 00lm: $l + 2m = 4n$, $hhlm$: $2h + l = 4n$, and hk00: $h = 2n$.

The commensurate and incommensurate phases are present as domains next to each other. This can be seen from the occurrence in the top inset of Figure 4a of the reflections at the centre of some pairs of satellites, which originate from domains of the commensurate phase.

In the earlier mentioned domains, where the q-vector has nonzero a^* and b^* components, the tetragonal symmetry is necessarily broken.[36-40] The tetragonal model deduced below for the single crystals was used for generating the calculated image shown as an inset in Figure 4e. It shows a good agreement for the basic feature seen in the image. However, small deviations for the atomic positions are present, which can be explained using the incommensurate model elaborated by Ye *et al.* for the NCL compound $MnSi_{2-x}$.[40] According to Ye *et al.*, the "orientation anomaly" is caused by systematic shifting of the helical arrangement of the metalloid atoms along the "chimney" in the transition metal sublattice. This effect can effectively be observed in the HAADF-STEM image in Figure 4d indicated by the white lines. The local variations in the q-vector are most likely due to local differences in chemical composition.[21,41] Using the formula proposed in Ref. [21], Ge/Fe = 2 - c^*_{Ge}/c^*_{Fe}, results in a composition $FeGe_{1.51(3)}$ for q = 0.49(3) c^*. Such deviations from the stoichiometric composition with γ = 1.5 are unfortunately too small to confirm with EDX analysis, as they are beyond the precision of EDX on a TEM instrument. In summary, two main phases appear in the polycrystalline sample of $FeGe_\gamma$ ($\gamma \approx 1.5$): (i) an orthorhombic commensurate structure with cell parameters $a \approx 5.45$ Å, $b \approx 5.6$ Å, and $c \approx 8.95$ Å and space group $Pcc2$ or $Pccm$; and (ii) an incommensurate phase that can be indexed with the superspace group used in literature for NCLs[35,36],

i.e. $I4_1/amd$:00ss, and with approximate cell parameters $a \approx 5.55$ Å, $c \approx 4.55$ Å, and variable q, most frequently $q = 0.49(3)\,c^*$. The patterns agree with the patterns characteristic of NCLs, however, the simultaneous presence of a commensurate and several slightly different incommensurate phases, and minor amounts of admixtures hinder fitting of the PXRD pattern of $FeGe_\gamma$ for $\gamma = 1.5$.

Crystal structure: single crystals

In the single-crystal X-ray experiments, the reciprocal space was carefully scanned in a search for the presence of superstructure reflections that would signify incommensurate modulation of the crystal structure. However, only reflections belonging to the undistorted conventional tetragonal unit cell were found. The data collected can be indexed in the primitive tetragonal unit cell with $a = 5.5848(8)$ Å and $c = 8.9400(18)$ Å. The P-4c2 space group (No. 116) was chosen on the basis of diffraction pattern symmetry and systematic extinction conditions. The crystal structure was solved by direct methods and refined against $|F^2|$. Details of the data collection at 100 K and structure refinement parameters are listed in Table 1, the atomic coordinates and selected interatomic distances are given in Tables 2 and 3, respectively.

Crystal structure solution and refinement show that the selected single crystals possess a normal commensurate chimney ladder structure. They are characterized by the stoichiometric composition Fe_2Ge_3, in contrast to polycrystalline $FeGe_\gamma$. Here, substantial difference between single-crystal and polycrystalline specimens appears, since the single crystals grown by chemical transport method do not show any indications of a crystal structure distortion or incommensurability that are observed in the case of polycrystalline $FeGe_\gamma$. Supposedly, it is the small size of crystallites that is responsible for the incommensurability, since small crystallites contain large amounts of imperfections in the crystal lattice, such as vacancies and dislocations, which are favorable for shifts of atoms from their ideal positions. In the case of single crystals rather the regular crystal structure is observed, in which a perfect match between the Fe and Ge sublattices yields non-distorted periodicity within a conventional unit cell of the Ru_2Sn_3-type.

A view of the crystal structure along the [001] and [100] directions is shown in Figure 5a. The crystal structure possesses the common feature of NCLs with Fe atoms forming the *β*-Sn-type arrangement of the condensed four-step helices aligned in the [001] direction. At the same time, Ge atoms are located within these helices of Fe atoms in the form of 3-step helices. The Fe and Ge atoms are arranged in a seemingly simple and rational way forming helices inside other helices. However, the coordination polyhedra of Fe atoms are rather complex. They can not be described in a simple way by comparing with conventional types of polyhedra. The coordination polyhedra of Fe atoms are presented in Figure 5b. Iron atoms in the Fe1 position have 6 short distances to the Ge atoms (Table 3) and are additionally connected via ~ 3.0 Å contacts to 2 Ge atoms and 4 Fe atoms, such that the coordination number of Fe1 increases from 6 to 12, when longer distances are considered. Similarly, each of the Fe2 and Fe3 atoms, in addition to the short Fe-Ge distances, possesses 4 other contacts of ~ 3.0 Å to Fe atoms. Thus, the Fe2 and Fe3 atoms can be assigned the coordination numbers of 10 and 12, respectively. The additional Fe-Fe contacts are from the Fe atoms within the 4-step helices of the *β*-Sn-type arrangement. Each Fe atom is connected with 4 other Fe atoms located at the distance of ~ 3.0 Å, and these Fe-Fe contacts are important when applying the modified 18-*n* rule to Fe_2Ge_3. Indeed, according to the 18-*n* rule[16], each Fe atom tends to form the closed 18-electron configuration through the regular *σ*-type Fe-Ge bonds. When there are exclusively Fe-Ge bonds, 18 valence electrons per Fe atom would be required to maintain the 18-electron configuration. At the same time, the formation of special Fe-Fe bonds, which have a multicenter nature involving Ge atoms, and which are isolobal to *σ*-type Fe-Fe bonds, reduces the required number of valence electrons to the value of 18-*n*, where *n* is the number of such Fe-Fe bonds. 4 Fe-Fe contacts per Fe atom are observed in the crystal structure of Fe_2Ge_3, hence, 14 valence electrons are required in order to achieve the 18-electron configuration. Therefore, Fe_2Ge_3 obeys the 18-*n* rule. The stability of this compound should be rooted in a pseudogap or even a real band gap in the vicinity of the Fermi energy as demonstrated below by electronic structure calculations.

Electronic structure

Crystal structure parameters were used to perform electronic structure calculations for Fe_2Ge_3 with the ideal chimney ladder structure of the Ru_2Sn_3-type. The calculated density of states, which is shown in the left panel of Figure 6, consists mainly of the Fe 3*d* and Ge 4*s* and 4*p* contributions. The 14 electron rule formulated for NCLs,[18] prior the 18-*n* rule was invented, is based exactly on this set of valence orbitals. The calculations confirm that the interaction of the Fe 3*d* with Ge 4*s* and 4*p* orbitals is responsible for the chemical bonding and leads to the formation of a narrow band gap. Analysis of partial contributions shows that the Fe 3*d* and Ge 4*p* states form the edges of the band gap (inset of Figure 6). The Ge 4*s* orbitals contribute significantly in the energy region between -13 eV and -7 eV only, forming the pocket of bonding states.

Band dispersion curves calculated for Fe_2Ge_3 are shown in the right panel of Figure 6. Here, a narrow band gap of 0.11 eV separating the valence and conduction bands is observed. The top of the valence band is formed by an almost parabolic maximum of the Ge 4*p* band located at the Γ point of the Brillouin zone. At the same time, the bottom of the conduction band consists mainly of the flat Fe 3*d* states with the minimum also located at the Γ point. It should be noted here that our results differ significantly from the data obtained by Sato *et al.*[22] who carried out optimization of the Fe_2Ge_3 structural parameters assuming the Ru_2Sn_3-type of crystal structure and performed calculations using the FP-LAPW PBE GGA approach. The latter calculations predict the value of a band gap of 0.2 eV, which is twice higher than the value calculated in our study using the experimental structure parameters obtained at 100 K. We also found different location of bands on the band dispersion curves plot.

Spin-polarized electronic structure calculations with the ferromagnetic and antiferromagnetic initial spin configurations converge to the non-magnetic state evidencing against the formation of local moments in Fe_2Ge_3 and confirming that the non-magnetic configuration is lowest in energy. In summary, our electronic structure calculations show that Fe_2Ge_3 is a non-magnetic direct band semiconductor, in which the excitation of electrons from the steep Ge 4*p* bands to the more atomic-like flat Fe

3*d* bands is observed. This flat character of the compact Fe 3*d* bands underlies the formation of sharp peaks of the density of states on the band edges and, therefore, high values of the Seebeck coefficient for Fe_2Ge_3. Thermoelectric performance of Fe_2Ge_3 was analyzed within the Boltzmann transport theory by Sato *et al.* who found the theoretical values of *S* as low as -250 μV/K at 500 K for the case of *n*-type doping.[22] In order to resolve the behavior of Fe_2Ge_3, its transport properties have been studied in this work. Unfortunately, we did not succeed in the preparation of single crystals that are large enough for the measurements, thus only polycrystalline samples were investigated. Transport properties were measured on polycrystalline samples of $FeGe_\gamma$ (γ = 1.5) that possess the incommensurately modulated structure in contrast to single crystalline Fe_2Ge_3 with the ideal chimney ladder structure.

Transport and magnetic properties

Temperature-dependent resistivity, Seebeck coefficient, and thermal conductivity are shown in Figure 7. Resistivity of $FeGe_\gamma$ decreases with increasing temperature, and the slope of the $\rho(T)$ curve changes significantly with temperature. Accordingly, three different temperature regimes can be found on the $\rho(T)$ curve (Figure 7a). The first is characterized by the fast drop of the resistivity when the temperature is increased from 2 K to ~ 100 K. In the second regime, between 100 K and 370 K, the resistivity is almost temperature-independent. Finally, in the third regime above 370 K, resistivity decreases again with increasing temperature following activation behavior. To interpret these complex features, we compare the $\rho(T)$ data measured for $FeGe_\gamma$ with the temperature-dependent resistivity of $FeGa_3$.[42] In the case of $FeGa_3$, which is a semiconducting intermetallic compound with a narrow band gap of 0.5 eV, the $\rho(T)$ curve is not following simple activation behavior too. Rather, the resistivity of $FeGa_3$ is influenced by the presence of impurity bands[43] that render the slope of the $\rho(T)$ curve. Analogous to $FeGa_3$, we assume the presence of impurity states located within the band gap of $FeGe_\gamma$ that promote electronic transport. Then, the first low-temperature regime reflects activation of charge carriers from the valence band to the impurity bands. The second, mid-temperature regime reflects saturation of the impurity bands, and the temperature-independent resistivity

is observed. Finally, when the impurity bands are filled, the activation of charge carriers to the conduction band is observed. The inset of Figure 7a shows the resistivity as the $ln\rho(1/T)$ plot. On this plot, the linear behavior is observed at high temperatures yielding E_g = 0.03 eV. This value is in qualitative agreement with the results of electronic structure calculations, which predict the gap of 0.11 eV for Fe_2Ge_3 with an ideal chimney ladder structure. The discrepancy may be caused by the well-known overestimate of the band gap in LDA calculations and by additional peculiarities of polycrystalline $FeGe_\gamma$ with its incommensurately modulated structure. Nevertheless, the observed linear slope on the $ln\rho(1/T)$ plot indicates that the semiconducting behavior is an inherent feature of both commensurate Fe_2Ge_3 and polycrystalline $FeGe_\gamma$. Such a behavior appears at high temperatures when impurity bands saturate.

The semiconducting behavior seen in the resistivity data is corroborated by the measurements of the Seebeck coefficient (Figure 7b). The Seebeck coefficient of $FeGe_\gamma$ is negative in the examined temperature range, while its absolute value gradually increases with increasing temperature reaching $|S|$ = 190 μV/K at T = 400 K. This value is not in agreement with the $S(T)$ data presented in Ref. [22] probably due to the difference in sample preparation routes. The measured $S(T)$ dependence is monotonic below T = 400 K, however, a broad minimum of S values is observed at higher temperatures $T \approx$ 600-620 K.[22] According to the empirical rule, the $S(T)$ dependence of a semiconductor should exhibit an extremum, at which the temperature is roughly corresponds to 1000 E_g, where the temperature is in K units, and E_g is in eV. According to this "1000 E_g" formula, the value of $E_g \sim$ 0.6 eV is supposed for $FeGe_\gamma$, which is not in agreement with the results of electronic structure calculations. In our opinion, the misfit comes from the large uncertainty of the "1000 E_g" formula.

When compared to simple metallic conductors that typically show absolute values of the Seebeck coefficient in the range of 5-20 μV/K, the values of $|S|$ for $FeGe_\gamma$ are significantly higher. Other T-E intermetallics, which are narrow-gap semiconductors, also exhibit high values of $|S|$ at elevated temperatures. For instance,

the values of $|S|$ = 400 μV/K, 180 μV/K, and 420 μV/K at 400 K were observed for $FeGa_3$, $RuGa_3$, and $OsGa_3$, respectively.[44] As a consequence, such intermetallic compounds can be used in high-temperature thermoelectric materials. For instance, solid solutions based on $RuIn_3$ exhibit high values of $|S|$, and the dimensionless figure-of-merit ZT = 0.8 was achieved at high temperatures for $RuIn_{3-y}Zn_y$ with y = 0.025.[7] The potential use of $FeGe_\gamma$ as a high-temperature thermoelectric material was considered by Sato *et al.*, who found by semi-empirical calculations that ZT values above 1.0 can be achieved in this material when the electron count is optimized.[22]

Another important feature of the polycrystalline $FeGe_\gamma$ that provides an additional path to high thermoelectric performance is the low glass-like thermal conductivity observed in the broad temperature range. In our study, the observed κ is not exceeding 1 W m^{-1} K^{-1} in the temperature range of 4-400 K (Figure 7b). Such a low thermal conductivity can be compared to that of skutterudites and thermoelectric clathrates. The concept of a phonon crystal, where heavy rattling atoms are placed in spacious cages leading to an effective phonon relaxation,[45] explains the low thermal conductivity of such materials as, for instance, in the $Yb_xCo_{2.5}Fe_{1.5}Sb_{12}$ skutterudite[46] and $R_8Ga_{16}Ge_{30}$ (R = Sr, Eu) clathrates[47]. Here, we can assume that complex features of the crystal structure, including its incommensurability, may also cause low thermal conductivity that was independently observed for $FeGe_\gamma$ in this study, and in the literature.[22]

Magnetic susceptibility $\chi(T)$ of Fe_2Ge_3 single crystals measured in the temperature range between 2 K and 300 K in 7 T magnetic field is presented in Figure 8. The susceptibility is temperature-independent within its error bar at temperatures above 50 K. Below ~50 K a small upturn of $\chi(T)$ is observed, which probably is due to the presence of tiny amounts of paramagnetic impurities. For the temperature dependence of magnetic susceptibility of Fe_2Ge_3, different scenarios can be proposed compared to other narrow-gap intermetallic semiconductors. For instance, $FeSb_2$ exhibits nearly temperature-independent magnetic susceptibility at low temperatures and thermally activated $\chi(T)$ at higher temperatures.[48] For FeSi, a combination of the Curie-Weiss paramagnetic and activated behavior is observed in a

wide temperature range.[4] Finally, $CrSb_2$ exhibits $\chi(T)$, which is very similar to that of $FeSb_2$,[48] but in contrast to its Fe-based analog, $CrSb_2$ orders antiferromagnetically below T_N = 273 K.[49] In the case of Fe_2Ge_3, the observed $\chi(T)$ is temperature-independent at T > 50 K and very low in magnitude, which is consistent with the scenario of a non-metallic system with relatively small concentration of charge carriers and without the preformed local magnetic moments. Thus, the experimental magnetic susceptibility of single crystals of Fe_2Ge_3 corroborates its narrow-gap semiconducting behavior deduced from the measurements of resistivity and by the electronic structure calculations.

Conclusions

Chemical transport approach was utilized to synthesize the Nowotny chimney ladder compound Fe_2Ge_3. With iodine as transport agent, polycrystalline samples of $FeGe_\gamma$ can be prepared on a par with other synthetic techniques. According to the TEM studies, the obtained samples of $FeGe_\gamma$ (γ = 1.5) possess both the commensurate and incommensurately modulated chimney ladder structures, significantly hindering the interpretation of the X-ray powder patterns. Combined use of I_2 and $Mo(CO)_6$ transport agents in the temperature gradient affords single crystals of the target compound to be grown for the first time, so that its crystal structure could be finally resolved. Remarkably, stoichiometric Fe_2Ge_3 features a commensurate chimney ladder structure of the Ru_2Sn_3-type. Using single-crystal data, we demonstrated that Fe_2Ge_3 obeys the 18-*n* rule formulated for the T-E intermetallic compounds, and electronic structure calculations qualify Fe_2Ge_3 as a narrow-gap semiconductor in compliance with the 18-*n* rule. Temperature-dependent resistivity and Seebeck coefficient measurements corroborate the semiconducting behavior. From activated behavior of the resistivity a band gap of 30 meV is estimated, and high absolute values of the Seebeck coefficient are observed at elevated temperatures. Along with substantially low thermal conductivity below 1 W m^{-1} K^{-1}, these observations place Fe_2Ge_3 in a class of prospective thermoelectric materials. The new synthetic route developed in our study should foster further optimization of thermoelectric performance in future studies of this interesting material.

Acknowledgements

The authors thank Dr. Sergey Kazakov and Oleg Tyablikov for their help with the PXRD experiments. V.Yu.V. appreciates the help of Dr. Sergey Dorofeev in provision and handling of the $Mo(CO)_6$ reagent. The work is supported by the Russian Science Foundation, grant No. 17-13-01033. V.Yu.V. appreciates the support from the European Regional Development Fund, project TK134. A.A.T. acknowledges financial support by the Federal Ministry for Education and Research under the Sofja Kovalevskaya Award of the Alexander von Humboldt Foundation. E.V.D. thanks the National Science Foundation, grant No. CHE-1152441.

[1] Häussermann, U.; Boström, M.; Viklund, P.; Rapp, Ö.; Björnängen, T. $FeGa_3$ and $RuGa_3$: Semiconducting Intermetallic Compounds. *J. Solid State Chem.* **2002**, *165*, 94-99.

[2] Bogdanov, D.; Winzer, K.; Nekrasov, I.A.; Pruschke, T. Electronic Properties of the Semiconductor $RuIn_3$. *J. Phys.: Condens. Matter* **2007**, *19*, 232202.

[3] Evers, J.; Dehlinger, G.; Meyer, H. Semiconducting Behavior of $RuGa_2$. *Mat. Res. Bull.* **1984**, *19*, 1177-1180.

[4] Paschen, S.; Felder, E.; Chernikov, M.A.; Degiorgi, L.; Schwer, H.; Ott, H.R.; Young, D.P.; Sarrao, J.L.; Fisk, Z. Low-Temperature Transport, Thermodynamic, and Optical Properties of FeSi. *Phys. Rev. B* **1997**, *56*, 12916.

[5] Petrovic, C.; Kim, J.W.; Bud'ko, S.L.; Goldman, A.I.; Canfield, P.C.; Choe, W.; Miller, G.J. Anisotropy and Large Magnetoresistance in the Narrow-Gap Semiconductor $FeSb_2$. *Phys. Rev. B* **2003**, *67*, 155205.

[6] Sales, B.C.; May, A.F.; McGuire, M.A.; Stone, M.B.; Singh, D.J.; Mandrus, D. Transport, Thermal, and Magnetic Properties of the Narrow-Gap Semiconductor $CrSb_2$. *Phys. Rev. B* **2012**, *86*, 235136.

[7] Wagner, M.; Cardoso-Gil, R.; Oeschler, N.; Rosner, H.; Grin, Yu. $RuIn_{3-x}Sn_x$, $RuIn_{3-x}Zn_x$, and $Ru_{1-y}In_3$ – New Thermoelectrics Based on the Semiconductor $RuIn_3$. *J. Mater. Res.* **2011**, *26*, 1886-1893.

[8] Kasinathan, D.; Wagner, M.; Koepernik, K.; Cardoso-Gil, R.; Grin, Yu.; Rosner, H. Electronic and Thermoelectric Properties of $RuIn_{3-x}A_x$ (A = Sn, Zn). *Phys. Rev. B* **2012**, *85*, 035207.

[9] Wagner-Reetz, M.; Kasinathan, D.; Schnelle, W.; Cardoso-Gil, R.; Rosner, H.; Grin, Yu. Phonon-Drag Effect in $FeGa_3$. *Phys. Rev. B* **2014**, *90*, 195206.

[10] Tomczak, J.M.; Haule, K.; Kotliar, G. Thermopower of the Correlated Narrow Gap Semiconductor FeSi and Comparison to RuSi. *NAPSB* **2013**, 45-57.

[11] Sun, P.; Oeschler, N.; Johnsen, S.; Iversen, B.B.; Steglich, F. Narrow Band Gap and Enhanced Thermoelectricity in $FeSb_2$. *Dalton Trans.* **2010**, *39*, 1012-1019.

[12] Shibayama, T.; Nohara, M.; Katori, H.A.; Okamoto, Y.; Hiroi, Z.; Takagi, H. Superconductivity in Rh_2Ga_9 and Ir_2Ga_9 without Inversion Symmetry. *J. Phys. Soc. Jpn.* **2007**, *76*, 073708.

[13] Xie, W.; Luo, H.; Phelan, B.F.; Klimczuk, T.; Cevallos, F.A.; Cava, R.J. Endohedral Gallide Cluster Superconductors and Superconductivity in $ReGa_5$. *PNAS* **2015**, *112*, 7048-7054.

[14] Verchenko, V.Yu.; Tsirlin, A.A.; Zubtsovskiy, A.O.; Shevelkov, A.V. Strong Electron-Phonon Coupling in the Intermetallic Superconductor Mo_8Ga_{41}. *Phys. Rev. B* **2016**, *93*, 064501.

[15] Yannello, V.J.; Kilduff, B.J.; Fredrickson, D.C. Isolobal Analogies in Intermetallics: The Reversed Approximation MO Approach and Applications to $CrGa_4$- and Ir_3Ge_7-Type Phases. *Inorg. Chem.* **2014**, *53*, 2730-2741.

[16] Yannello, V.J.; Fredrickson, D.C. Orbital Origins of Helices and Magic Electron Counts in the Nowotny Chimney Ladders: the 18-*n* Rule and a Path to Incommensurability. *Inorg. Chem.* **2014**, *53*, 10627-10631.

[17] Yannello, V.J.; Fredrickson, D.C. Generality of the 18-*n* Rule: Intermetallic Structural Chemistry Explained through Isolobal Analogies to Transition Metal Complexes. *Inorg. Chem.* **2015**, *54*, 11385-11398.

[18] Fredrickson, D.C.; Lee, S.; Hoffmann, R. The Nowotny Chimney Ladder Phases: Whence the 14 Electron Rule? *Inorg. Chem.* **2004**, *43*, 6159-6167.

[19] Fredrickson, D.C.; Lee, S.; Hoffmann, R.; Lin, J. The Nowotny Chimney Ladder Phases: Following the c_{pseudo} Clue toward an Explanation of the 14 Electron Rule. *Inorg. Chem.* **2004**, *43*, 6151-6158.

[20] Gerasimov, K.B.; Pavlov, S.V. New Equilibrium Phase in the Fe-Ge System Obtained by Mechanical Alloying. *Intermetallics* **2000**, *8*, 451-452.

[21] Li, W.; Li, Y.; Ma, X.; Zhang, Z. Incommensurate Structure of a New Nowotny Phase in Fe-Ge System. *Mater. Chem. Phys.* **2014**, 148, 490-493.

[22] Sato, N.; Ouchi, H.; Takagiwa, Y.; Kimura, K. Glass-like Lattice Thermal Conductivity and Thermoelectric Properties of Incommensurate Chimney-Ladder Compound $FeGe_\gamma$. *Chem. Mater.* **2016**, 28, 529-533.

[23] Bruker 2015. SADABS v. 2014/5. Bruker AXS Inc., Madison, Wisconsin, USA.

[24] Sheldrick, G.M. Crystal Structure Refinement with SHELXL. *Acta Cryst.* **2015**, *C71*, 3-8.

[25] Lobato, I.; Van Dyck, D. MULTEM: A new multislice program to perform accurate and fast electron diffraction and imaging simulations using Graphics Processing Units and CUDA. *Ultramicroscopy* **2015**, *156*, 9-17.

[26] Koepernik, K.; Eschrig, H. Full-Potential Nonorthogonal Local-Orbital Minimum-Basis Band-Structure Scheme. *Phys. Rev. B* **1999**, *59*, 1743.

[27] Perdew, J.P.; Wang, Y. Accurate and Simple Analytic Representation of the Electron-Gas Correlation Energy. *Phys. Rev. B* **1992**, 45, 13244.

[28] Blöchl, P.E.; Jepsen, O.; Andersen, O.K. Improved Tetrahedron Method for Brillouin-Zone Integrations. *Phys. Rev. B* **1994**, *49*, 16223.

[29] Okamoto, H. Fe-Ge (Iron-Germanium). *JPEDAV* **2008**, 29:292.

[30] Richardson, M. The Partial Equilibrium Diagram of the Fe-Ge System in the Range 40-72 at. % Ge, and the Crystallization of Some Iron Germanides by Chemical Transport Reactions. *Acta Chem. Scand.* **1967**, *21*, 2305-2317.

[31] Schäfer, H.; Hönes, W.J. Das gasförmige Eisen(III)-jodid und die Gleichgewichte im System Eisen-Jod. *Z. anorg. allg. Chem.* **1956**, *288*, 62-80.

[32] Ferguson, I.F.; Ainscough, J.B.; Morse, D.; Miller, A.W. Decomposition of Molybdenum Hexacarbonyl. *Nature* **1964**, *202*, 1327-1328.

[33] Schwomma, O.; Nowotny, H.; Wittmann, A. Untersuchungen im System: Ru-Sn. *Monatsh. Chem.* **1964**, *95*, 1538-1543.

[34] Pushcharovskii, D.Y.; Parthé, E. The Orthorhombic Crystal Structure of Ru_2Si_3, Ru_2Ge_3, Os_2Si_3 and Os_2Ge_3. *Acta Crystallogr. B* **1974**, *30*, 2692-2696.

[35] Rohrer, F.E.; Lind, H.; Eriksson, L.; Larsson, A.-K.; Lidin, S. Incommensurately Modulated Nowotny Chimney-Ladder Phases: $Cr_{1-x}Mo_xGe_{\sim 1.75}$ with x = 0.65 and 0.84. *Z. Kristallogr.* **2001**, *216*, 190-198.

[36] Rohrer, F.E.; Lind, H.; Eriksson, L.; Larsson, A.-K.; Lidin, S. On the Question of Commensurability – The Nowotny Chimney-Ladder Structures Revisited. *Z. Kristallogr.* **2000**, *215*, 650-660.

[37] De Ridder, R.; Van Tendeloo, G.; Amelinckx, S. Incommensurate Superstructures in $MnSi_{2-x}$. *Phys. Stat. Sol.* **1975**, *30*, 99-101.

[38] De Ridder, R.; Van Tendeloo, G.; Amelinckx, S. Electron Microscopy Study of Chimney Ladder Structures $MnSi_{2-x}$ and $MoGe_{2-x}$. *Phys. Stat. Sol.* **1976**, *33*, 383-393.

[39] De Ridder, R.; Amelinckx, S. The Structure of Defect Manganese Silicides. *Mat. Res. Bull.* **1971**, *6*, 1223-1234.

[40] Ye, H.Q.; Amelinckx, S. High-Resolution Electron Microscopic Study of Manganese Silicides $MnSi_{2-x}$. *J. Solid State Chem.* **1986**, *61*, 8-39.

[41] Lu, G.; Lee, S.; Lin, J.; You, L.; Sun, J.; Schmidt, J.T. $RuGa_vSn_w$ Nowotny Chimney Ladder Phases and the 14-Electron Rule. *J. Solid State Chem.* **2002**, *164*, 210-219.

[42] Hadano, Y.; Narazu, S.; Avila, M.A.; Onimaru, T.; Takabatake, T. Thermoelectric and Magnetic Properties of a Narrow-Gap Semiconductor $FeGa_3$. *J. Phys. Soc. Jpn.* **2009**, *78*, 013702.

[43] Gippius, A.A.; Verchenko, V.Yu.; Tkachev, A.V.; Gervits, N.E.; Lue, C.S.; Tsirlin, A.A.; Büttgen, N.; Krätschmer, W.; Baenitz, M.; Shatruk, M.; Shevelkov, A.V. Interplay between Localized and Itinerant Magnetism in Co-Substituted $FeGa_3$. *Phys. Rev. B* **2014**, *89*, 104426.

[44] Amagai, Y.; Yamamoto, A.; Lida, T.; Takanashi, Y. Thermoelectric Properties of Semiconductorlike Intermetallic Compounds $TMGa_3$ (TM = Fe, Ru, and Os). *J. Appl. Phys.* **2004**, *96*, 5644-5648.

[45] Nolas, G.S. The Physics and Chemistry of Inorganic Clathrates. Springer Series in Materials Science; Springer Netherlands: Dordrecht, 2014; pp.169-191.

[46] Dong, Y.; Puneet, P.; Tritt, T.M.; Nolas, G.S. Crystal Structure and High Temperature Transport Properties of Yb-Filled *p*-Type Skutterudites $Yb_xCo_{2.5}Fe_{1.5}Sb_{12}$. *J. Solid State Chem.* **2014**, *209*, 1-5.

[47] Cohn, J.L.; Nolas, G.S.; Fessatidis, V.; Metcalf, T.H.; Slack, G.A. Glasslike Heat Conduction in High-Mobility Crystalline Semiconductors. *Phys. Rev. Lett.* **1999**, *82*, 779.

[48] Hu, R.; Mitrovic, V.F.; Petrovic, C. Anisotropy in the magnetic and electrical transport properties of $Fe_{1-x}Cr_xSb_2$. *Phys. Rev. B* **2007**, *76*, 115105.

[49] Stone, M.B.; Lumsden, M.D.; Nagler, S.E.; Singh, D.J.; He, J.; Sales, B.C.; Mandrus, D. Quasi-One-Dimensional Magnons in an Intermetallic Marcasite. *Phys. Rev. Lett.* **2012**, *108*, 167202.

Table 1. Crystal data collection and refinement details for Fe_2Ge_3 at 100 K.

Parameter	value
Formula	Fe_2Ge_3
formula weight (g mol^{-1})	329.47
crystal size (mm)	0.04×0.06×0.12
crystal system	tetragonal
space group	*P*-4*c*2 (No. 116)
a (Å)	5.5848(8)
c (Å)	8.9400(18)
V (Å^3)	278.84(10)
Z	4
ρ_{calc} (g cm^{-3})	7.848
μ (mm^{-1})	41.773
temperature (K)	100
radiation, λ (Å)	(Mo Kα) 0.71073
absorption correction	multi-scan
structure solution	direct methods
refinement	against $\|F^2\|$
θ range (°)	3.65-36.30
index ranges	$-9 \le h \le 9$
	$-9 \le k \le 9$
	$-14 \le l \le 14$
N collected	15306
N unique	685
N observed [$I > 2\sigma(I)$]	674
number of parameters	26
R_1 [$I > 2\sigma(I)$]	0.0276
wR_2 [$I > 2\sigma(I)$]	0.0691
GOF	1.357
residual peaks (ē Å^{-3})	1.785/-1.951

Table 2. Atomic coordinates and thermal displacement parameters for the crystal structure of Fe_2Ge_3 at 100 K.

atom	site	*x*	*y*	*z*	U_{eq} (Å^2)
Fe1	4*i*	0	1/2	0.12591(18)	0.0022(2)
Fe2	2*b*	1/2	1/2	1/4	0.0029(3)
Fe3	2*c*	0	0	0	0.0022(3)
Ge1	8*j*	0.65469(14)	0.22012(16)	0.08497(12)	0.00606(17)
Ge2	4*f*	0.17682(13)	0.17682(13)	1/4	0.00242(18)

Table 3. Selected interatomic distances in the structure of Fe_2Ge_3 at 100 K.

Bond		Distance (Å)
Fe1	–Ge1 (2×)	2.4107(16)
	–Ge1 (2×)	2.5092(9)
	–Ge2 (2×)	2.3374(9)
	–Fe2 (2×)	3.0047(8)
	–Fe3 (2×)	3.0108(8)
Fe2	–Ge1 (4×)	2.3165(10)
	–Ge2 (2×)	2.5525(11)
	–Fe1 (4×)	3.0047(8)
Fe3	–Ge1 (4×)	2.4098(9)
	–Ge2 (4×)	2.6354(7)
	–Fe1 (4×)	3.0108(8)
Ge2	–Ge1 (2×)	2.8243(10)
	–Ge2 (1×)	2.793(2)

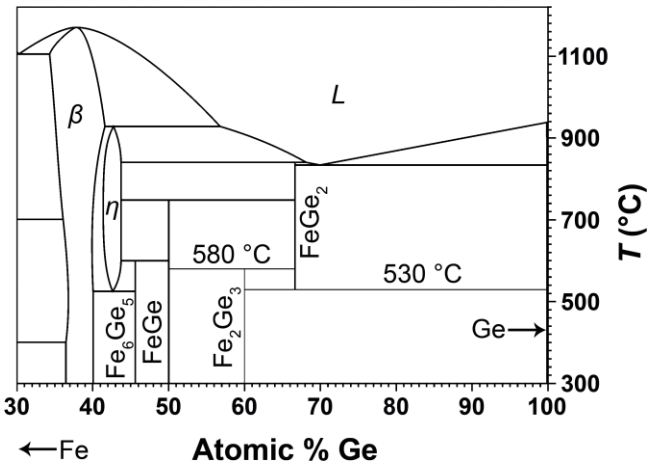

Fig. 1. Part of the Fe-Ge phase diagram with Ge concentrations of > 30 at.%.

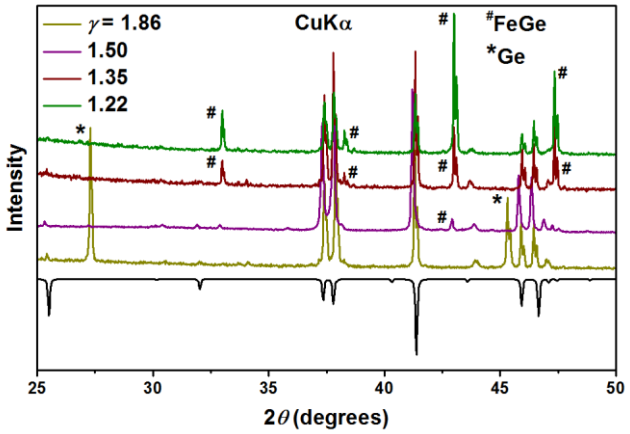

Fig. 2. PXRD patterns of $FeGe_\gamma$ alloys near the stoichiometric composition of γ = 1.5. Peak positions of FeGe ($P2_13$, FeSi-type) and Ge phases are marked with hash marks and asterisks, respectively. Black line at the bottom display the theoretical PXRD pattern of Fe_2Ge_3 with the commensurate Ru_2Sn_3-type crystal structure (for more details, see the section **Crystal structure: single crystals**).

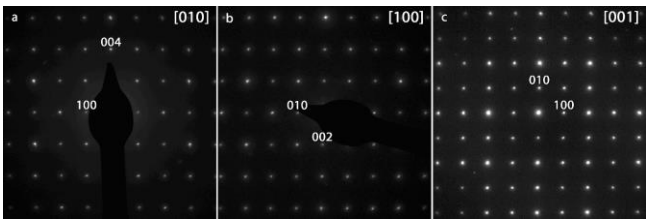

Fig. 3. SAED patterns taken along [010], [100], and [001] directions for the commensurate orthorhombic phase.

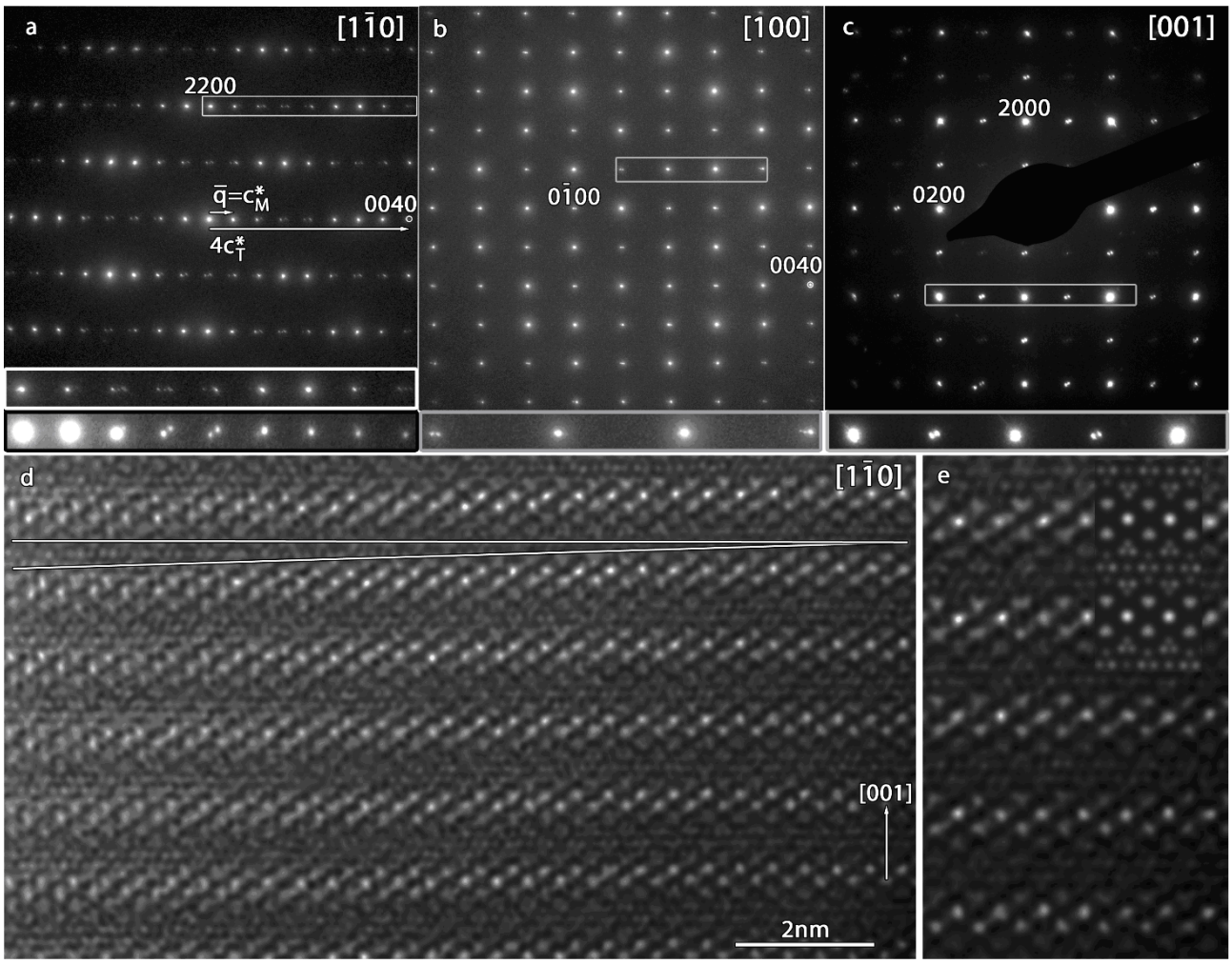

Fig. 4. (a)-(c) Representative SAED patterns of $FeGe_{\gamma}$ along the [1-10], [100] and [001] directions for the incommensurately modulated phase. The insets show enlargements of the parts indicated on the figures, except the inset indicated by a black border, which is an enlargement of an SAED pattern from another crystal for comparison. (d) HAADF-STEM image of a typical $FeGe_{\gamma}$ crystal. The white lines indicate the shift of the Ge helices in successive Fe chimneys. (e) Enlarged view of (d), including an image calculated using the model found for the Fe_2Ge_3 single crystal structure (for more details, see the section **Crystal structure: single crystals**). Slight differences are visible due to the incommensurate character of $FeGe_{\gamma}$.

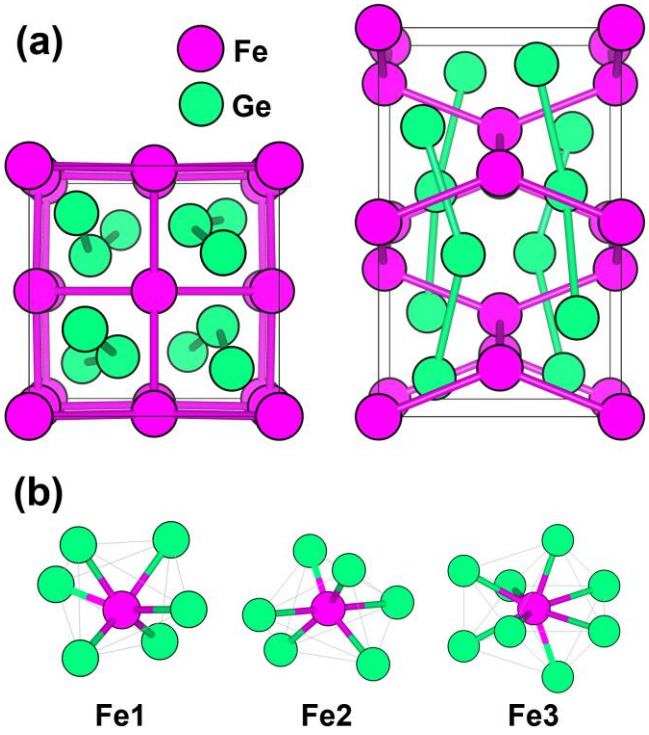

Fig. 5. (a) View of the Fe_2Ge_3 crystal structure along the [001] (left) and [100] (right) directions. (b) Coordination polyhedra of Fe atoms.

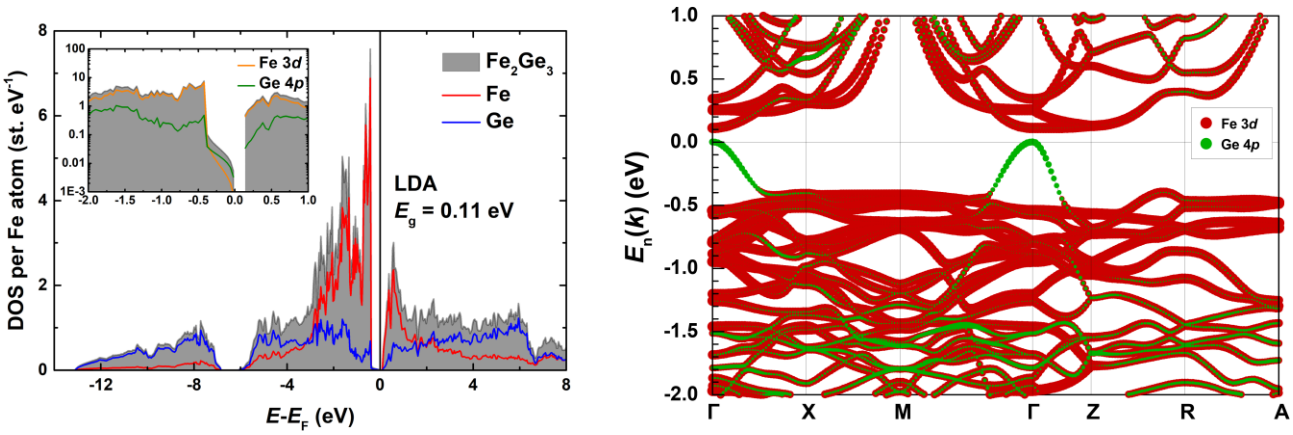

Fig. 6. (Left) Density of states plot calculated for Fe_2Ge_3. The contributions of Fe and Ge species are represented by the red and blue lines, respectively. The inset shows the region near the Fermi energy. On the inset, the contributions of the Fe 3*d* and Ge 4*p* states are shown in orange and green colors, respectively. (Right) Electronic structure of Fe_2Ge_3 as obtained with the PW LDA. Partial contribution of the Fe 3*d* states is shown in red color, and that of Ge 4*p* states – in green color.

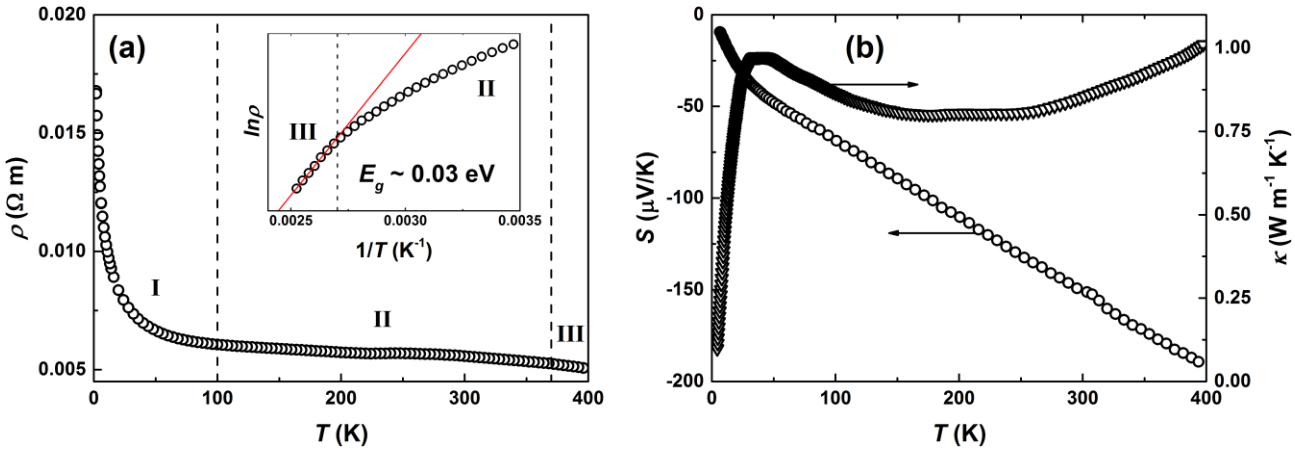

Fig. 7. (a) Temperature-dependent resistivity of $FeGe_\gamma$ (γ = 1.5). The inset shows resistivity as the $ln\rho(1/T)$ plot, the red line represents a linear fit to the data. (b) Seebeck coefficient and thermal conductivity of $FeGe_\gamma$ (γ = 1.5).

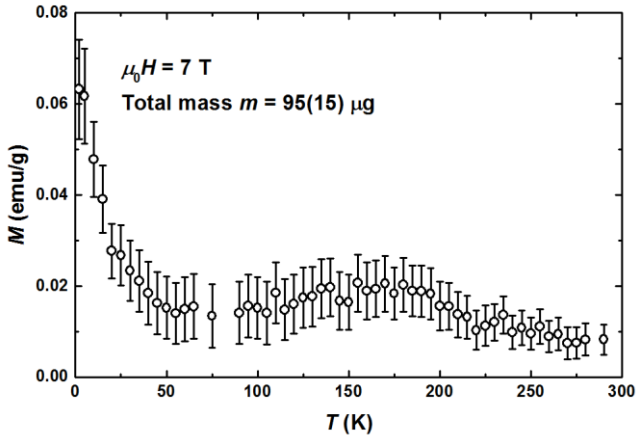

Fig. 8. Magnetic susceptibility of Fe_2Ge_3 single crystals measured in 7 T magnetic field.

TOC graphic